Water Resources Research

Supporting Information for

Evaporation and water sourcing dominate lake and stream isotopic variability across time and space in a High Arctic periglacial landscape

Pete D. Akers[1], Ben G. Kopec[2], Eric S. Klein[3], Jeffrey M. Welker[2,4,5]

[1]Discipline of Geography, School of Natural Sciences, Trinity College Dublin, Dublin, Ireland.

[2]Ecology and Genetics Research Unit, University of Oulu, 90014 Oulu, Finland.

[3]Department of Geological Sciences, University of Alaska Anchorage, Anchorage, AK, USA.

[4]Department of Biological Sciences, University of Alaska Anchorage, Anchorage, AK, USA.

[5]University of the Arctic (UArctic), c/o University of Lapland, 96101 Rovaniemi, Finland.

Contents of this file

Additional Supporting Information (Files uploaded separately)

Figure S1

Introduction

This supporting information contains figures and tables that provide additional visual and numerical context to the main text. Data and code used to produce these figures and tables are listed under the Availability Statement. All photographs in figures were taken by Pete D. Akers.

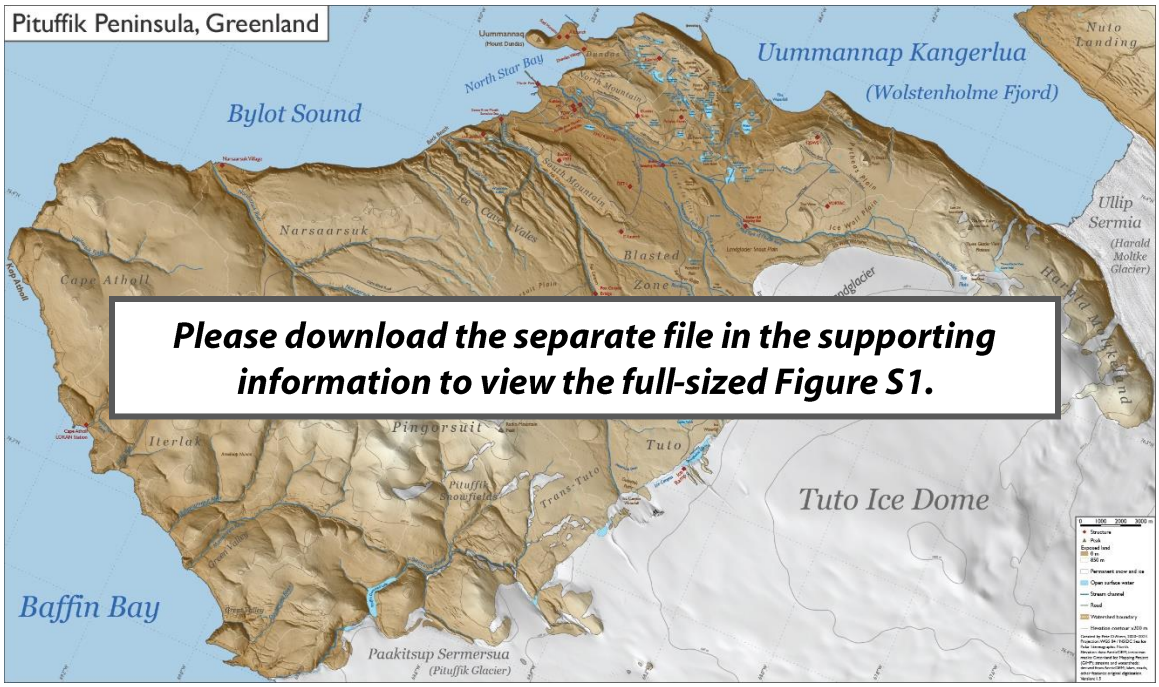

Figure S1 (Separate file). Poster-sized map of the hydrology and land features of the Pituffik Peninsula. Data used to create the map were taken from the Pituffik geospatial database (Akers et al., 2023b) and the cited data within that database. The map was created in QGIS and aesthetic modifications were made using Adobe Illustrator.

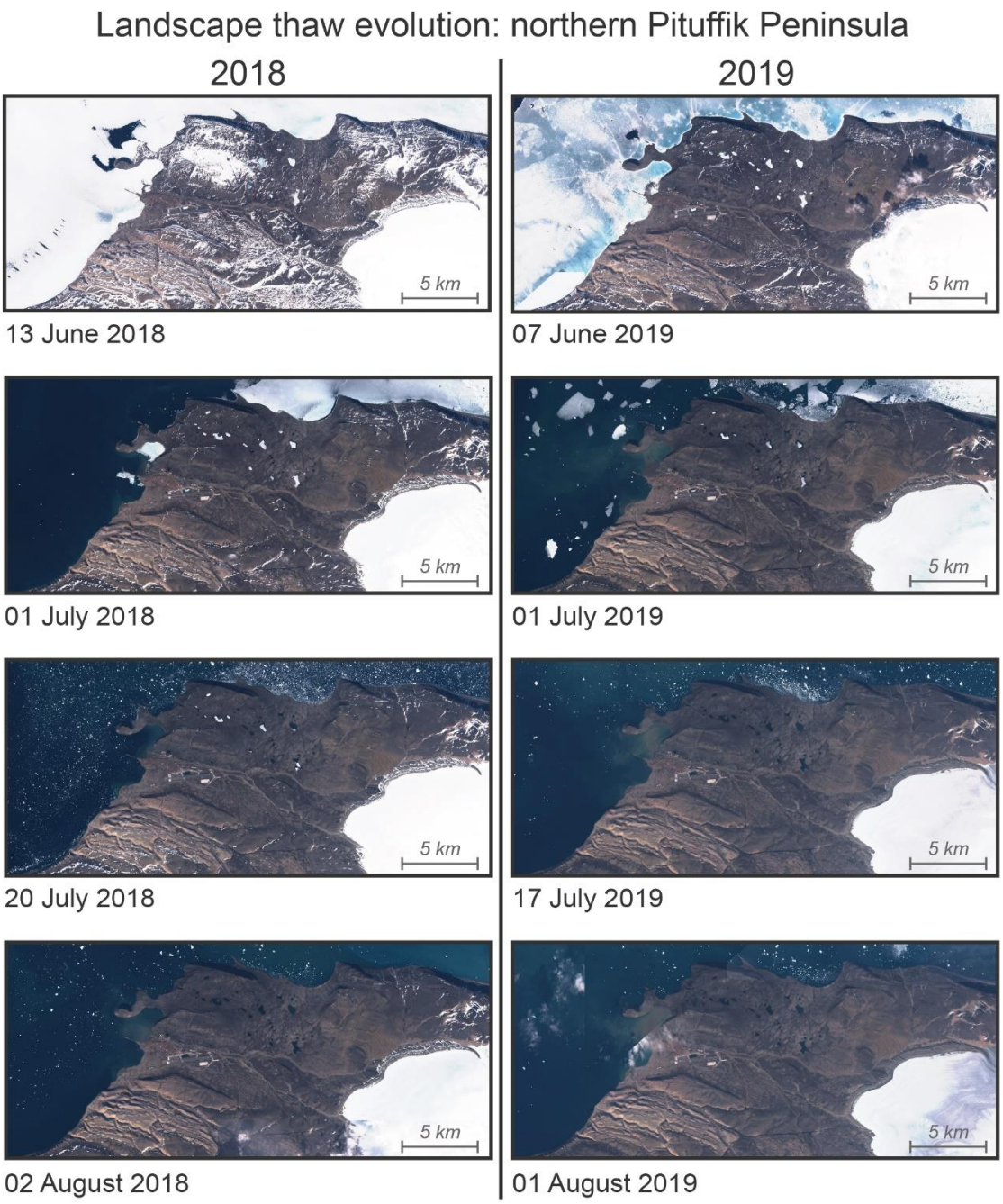

Figure S2. The general thawing progression of the northern Pituffik Peninsula landscape in summers 2018 and 2019. Pituffik Space Base is located at slightly left of direct center, and the Tuto ice dome of the GrIS is present at bottom right. Photographs on the same row are matched by date across the two years, although frequent cloud cover and fog limited same day comparisons in most cases. Note that snow on the landscape and lake ice lasted later into the summer in 2018 than 2019. Additionally, dark GrIS ice is visible in the 01 August 2019 image after an extreme surface melt event of the GrIS removed its snow cover and exposed the underlaying, less reflective ice.

Figure S3. Observed variability in stream flow rates in Pituffik streams in 2018 and 2019. In a), a moderate flow of the Pituffik River occurs in early summer due to melting of the tundra snowpack. In b) the Pituffik River discharges at near maximum rates due to an extreme GrIS surface melt event. For the Sioraq River, flow rates were moderate in early July 2018 under cool conditions and limited GrIS melt (c), but the same site is seen with very high flow on 01 August 2019 (d) during the same extreme GrIS surface melt event as (b). The Amitsuarsuk River has its highest flow rates in early summer when the tundra snowpack melts (not pictured) with lower flows sustained over the rest of summer (e) through precipitation, active layer water thaw, and residual snow patch melt. In contrast to the Pituffik and Sioraq Rivers (b, d), the Amitsuarsuk River's flow was very low during the 2019 extreme GrIS surface melt event (f) as the stream has no connection to the GrIS, and the lack of precipitation and strong evaporation during the 2019 summer suppressed its water supply.

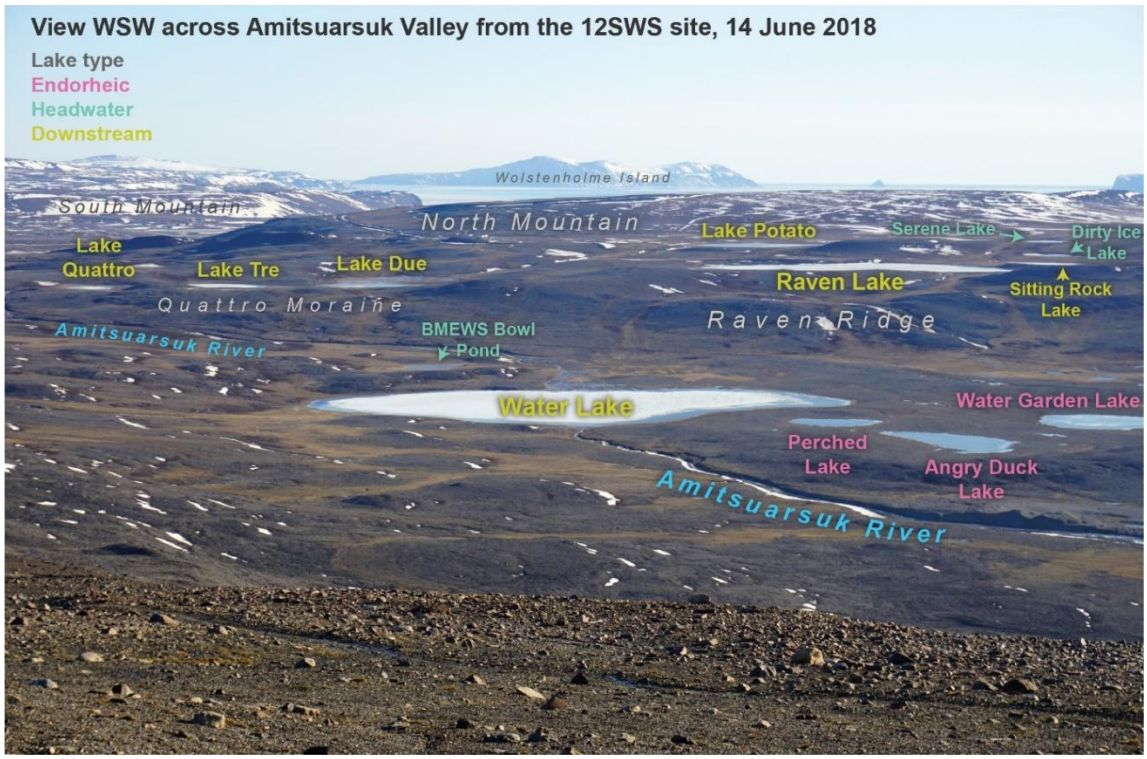

Figure S1. View of the Pituffik landscape and hydrological system around the Amitsuarsuk Valley. Visible lakes are labeled and colored according to their lake type. On the date of the photograph (14 Jun 2018), the tundra snowpack had only recently experienced substantial melt, and most lakes had only started to lose their ice cover. Note, however, that the shallower endorheic and headwater lakes are largely ice-free, likely due to earlier melt of their bedfast ice.

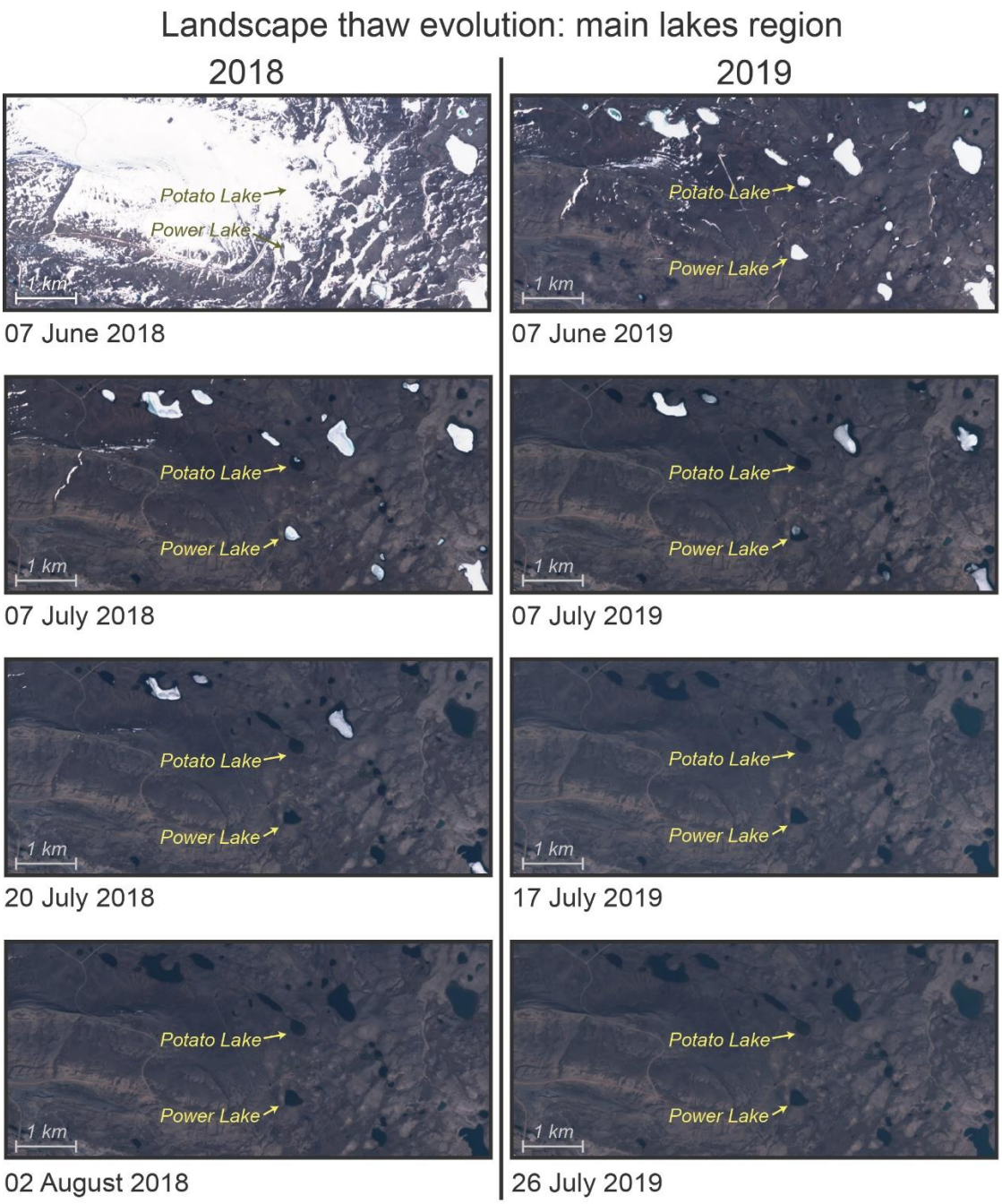

Figure S5. The general thawing progression of part of the main lakes region of the Pituffik Peninsula landscape in summers 2018 and 2019. The two frequently sampled lakes of Potato Lake and Power Lake are indicated, and other lakes can be identified through the main text's Figure 1. Photographs on the same row are matched by date across the two years, although frequent cloud cover and fog limited same day comparisons in some cases. Note that snow on the landscape and lake ice lasted later into the summer in 2018 than 2019.

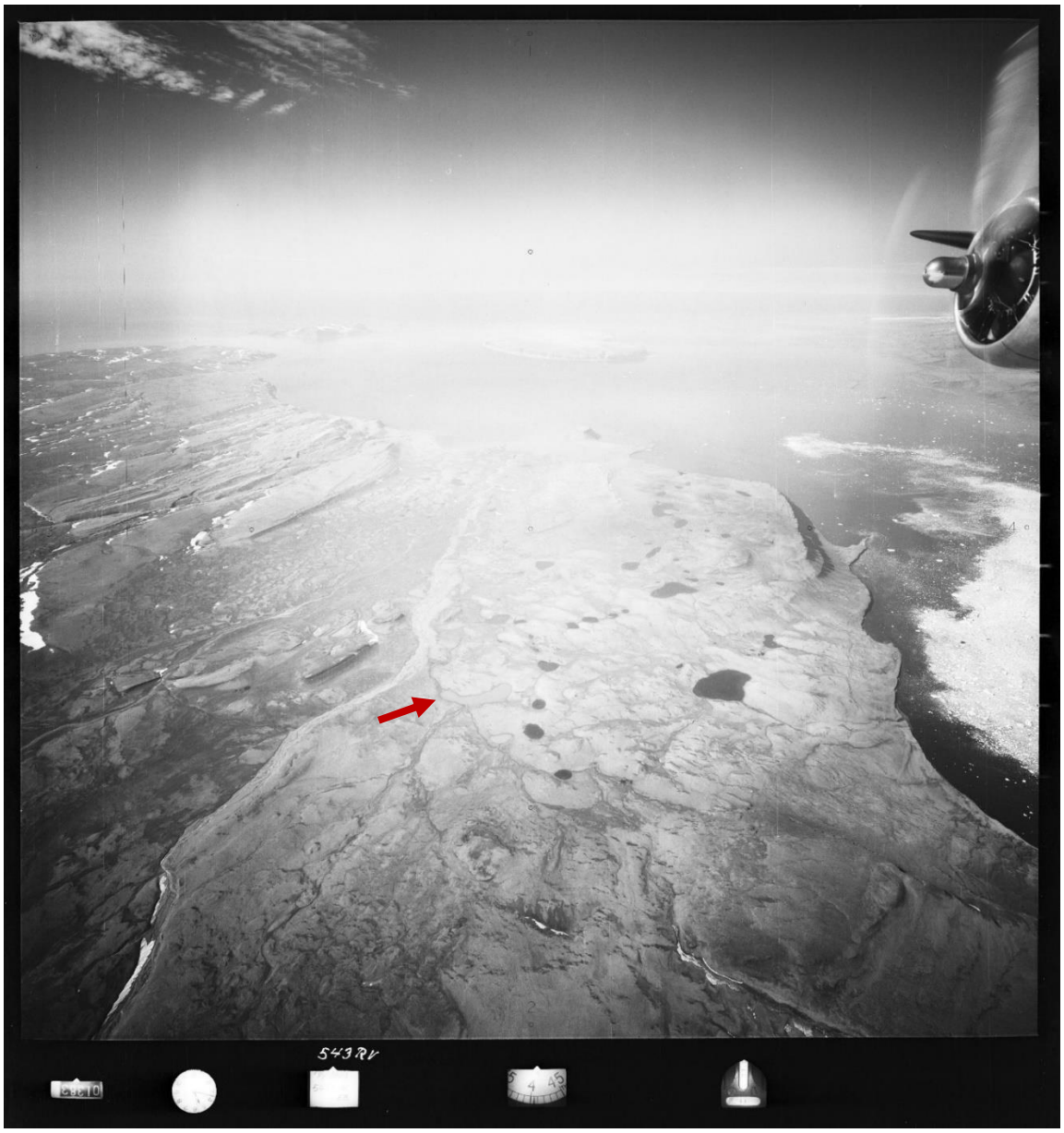

Figure S6. Aerial photograph of the main lakes region of Pituffik taken on 15 July 1949. This photograph is one of several taken on route 543RV and archived online by the Danish Agency for Data Supply and Infrastructure (Historiske Kort, 2023). The view here looks west along the northern coast of the Pituffik Peninsula from a point near the northern Tuto ice dome margin. Uummannaq can be seen just above the photograph's center, and the future Pituffik Space Base and runway will be located in the broad valley slightly left of image center. At the date this photograph was taken, the landscape and hydrology had not been significantly altered yet by humans. Of particular interest is the as-yet undammed Lake Crescent indicated by the red arrow with a notably lighter color than most other lakes in the image.

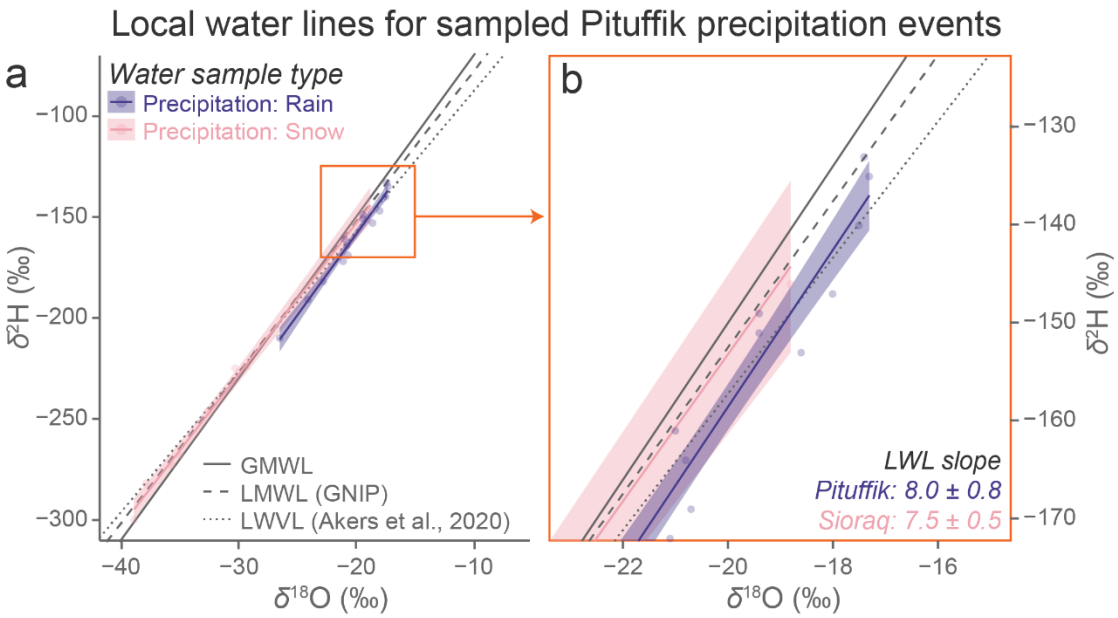

Figure S7. Local water line (LWL) linear regressions between $\delta^{18}O$ and $\delta^{2}H$ for sampled Pituffik precipitation events. Regressions are split between rain and snow events, and the 95% confidence intervals of the regressions are shaded. The global meteoric water line (GMWL, solid gray), local meteoric water line (LMWL, dashed gray) based on GNIP data (IAEA/WMO, 2022), and local water vapor line (LWVL, dotted gray) (Akers et al., 2020) are shown for reference. The plot in (b) is a magnified version of the area indicated with the orange square in (a) and matches the extent shown in the main manuscript's Figure 2c. LWL slope values and 95% confidence intervals of the slope are given at lower right.

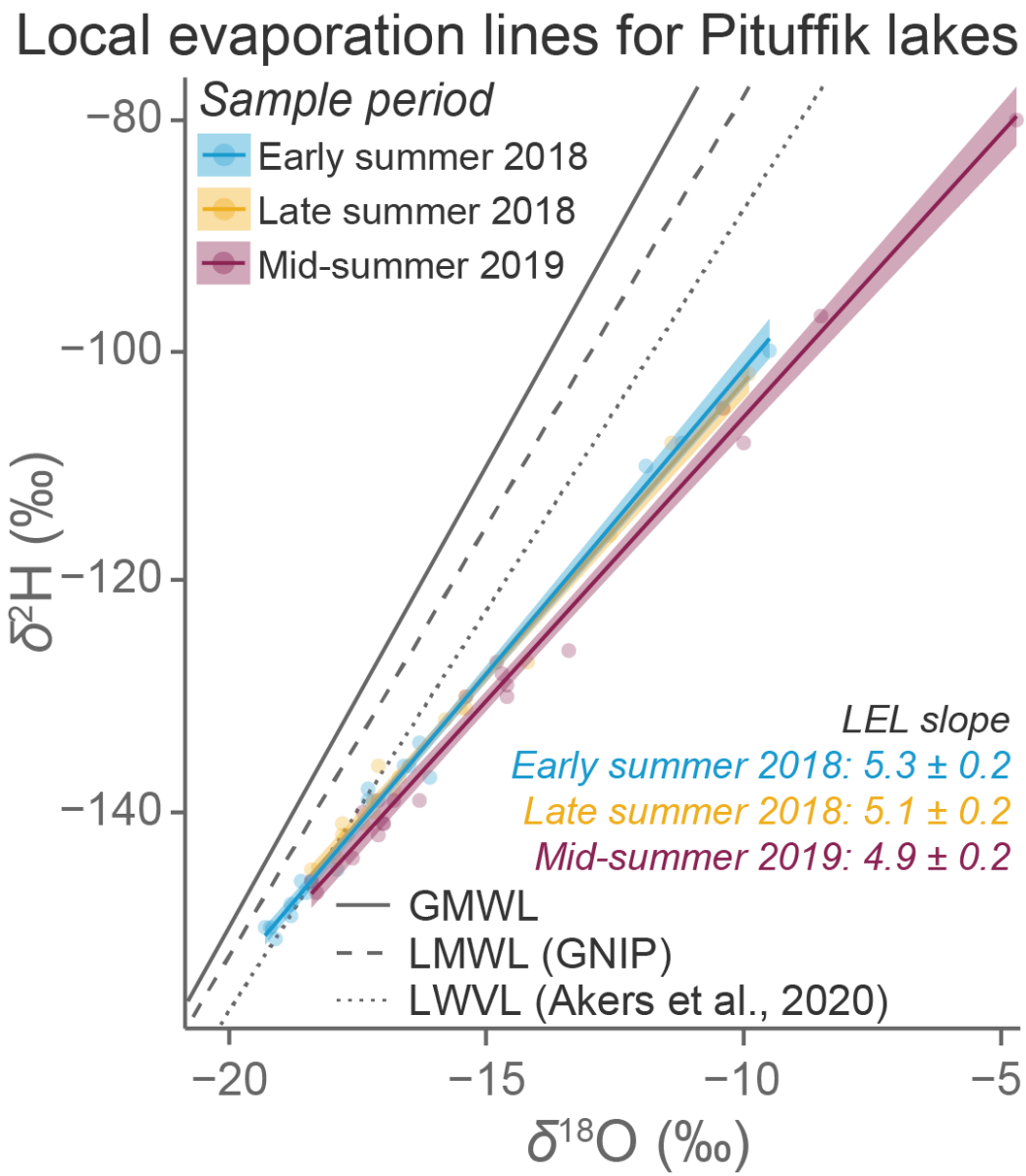

Figure S8. Linear regressions of δ^2H vs. $\delta^{18}O$ to display local evaporation lines (LELs) for Pituffik lakes by sampling period. Lake data is restricted to the subset of 18 lakes and 2 pools sampled in all three sampling periods. Each LEL represents a single sampling period and incorporates the isotopic values of all 18 lakes and 2 pools sampled during the period. LEL slope values and 95% confidence intervals of the slope are given for each sampling period at lower right. The global meteoric water line (GMWL, solid gray), local meteoric water line (LMWL, dashed gray) based on GNIP data (IAEA/WMO, 2022), and local water vapor line (LWVL, dotted gray) (Akers et al., 2020) are shown for reference.

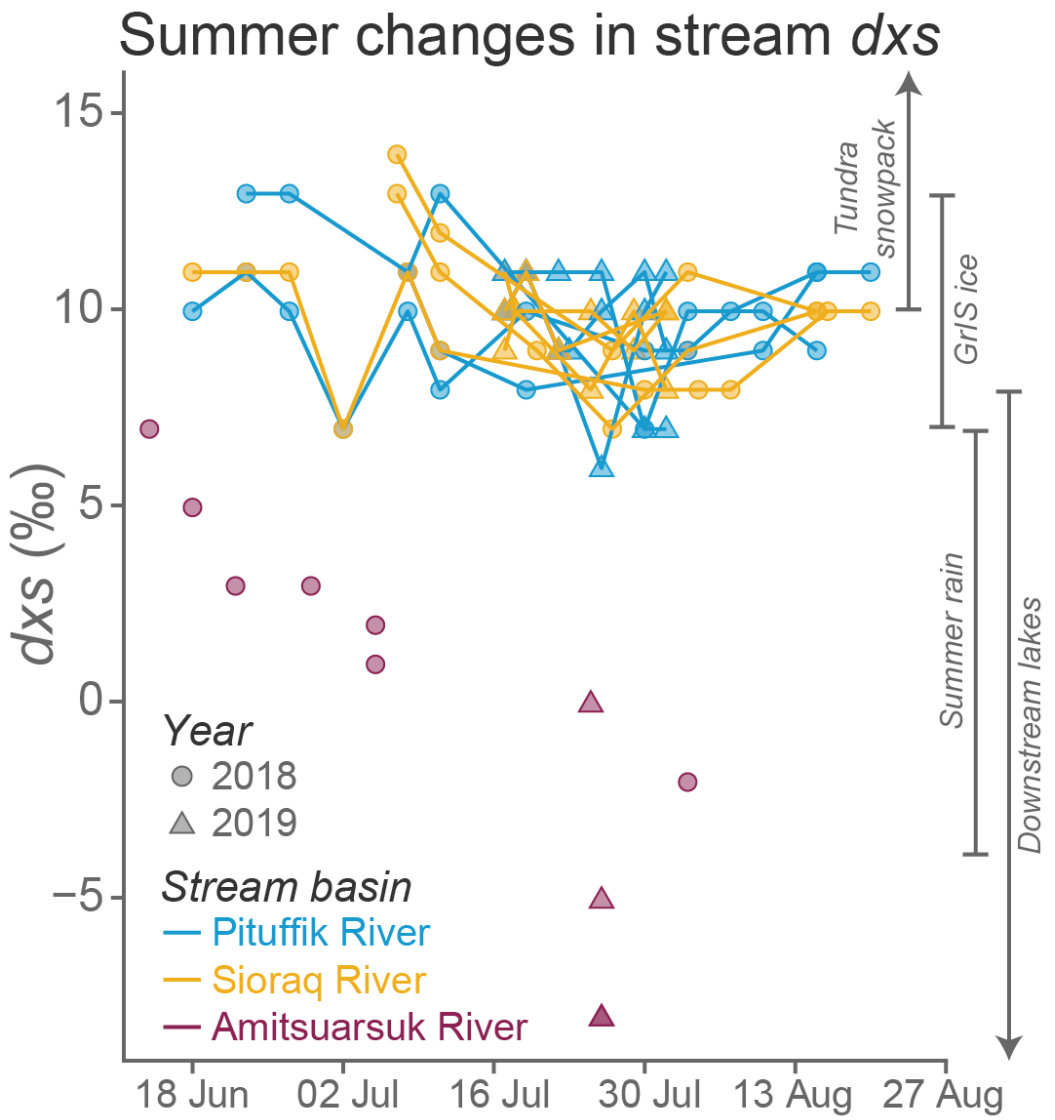

Figure S9. Evolution of Pituffik stream *dxs* values over the summer season. Samples were taken at three specific sites each along the Pituffik and Sioraq Rivers and at irregular sites along the Amitsuarsuk River. Lines connect the time-series for Pituffik and Sioraq River sites, but not for the Amitsuarsuk River because its samples were not consistently taken at the same site and thus are not a true comparable single-site time-series. Icons and lines are colored according to their stream basin. Samples from both 2018 (circles) and 2019 (triangles) are plotted by their date sampled. The *dxs* values of samples taken of the winter tundra snowpack, GrIS ice, summer rain events, and lakes with the downstream lake type are plotted at right for broader environmental context.

Table S1. Linear regression parameters for water δ^2H vs. $\delta^{18}O$ by sample type. Parameters for three isotopic reference lines are given at top: the global meteoric water line (GMWL) (Craig, 1961), the local meteoric water line (LMWL) based on monthly GNIP data taken at Thule Airport between 1966 and 1971 (IAEA/WMO, 2022), and the local water vapor line (LWVL) based on 10 min water vapor data sampled at South Mountain, Pituffik Space Base, between 2017 and 2020 (Akers et al., 2020). Parameters are given as 95% confidence intervals.

Reference line	**n**	**Slope**	**Intercept (‰)**	**r^2**
GMWL	–	8.0	+10	–
LMWL (GNIP)	42	7.5±0.4	−3±9	0.98
LWVL	147301	6.9±0.0	−18±0	0.98
Pituffik sample type				
Lake	161	5.0±0.2	−54±3	0.96
Pool	49	4.6±0.3	−63±6	0.94
Stream	121	6.2±0.3	−28±6	0.93
Surface flow	75	5.9±0.5	−36±10	0.87
Snow/ice	87	6.8±0.3	−15±7	0.95
Precipitation: rain	14	8.0±0.8	+2±16	0.97
Precipitation: snow	8	7.5±0.5	−3±16	0.99

Table S2. Results from the multiple regression and LASSO regression of lake water isotopic composition and environmental parameters. Lake sample set analyzed includes the 42 headwater and downstream lakes sampled in mid-summer 2019 and located in the main lake region north of the air base. Note that surface area was not included in the δ^2H multiple regression due to lack of importance and that LASSO regression did not find surface area or elevation to be important for δ^2H. Uncertainties are given as ± 1 standard error.

	$\delta^{18}O$		δ^2H		*dxs*	
Multiple regression parameter	**Coefficient (‰)**	**p-value**	**Coefficient (‰)**	**p-value**	**Coefficient (‰)**	**p-value**
Surface area (log)	-0.39 ± 0.16	0.02	–	–	2.9 ± 0.5	<<0.001
Watershed area (log)	-0.62 ± 0.13	<<0.001	-3.8 ± 0.6	<<0.001	1.2 ± 0.4	0.002
Elevation	-0.015 ± 0.004	<<0.001	-0.068 ± 0.023	0.006	0.052 ± 0.011	<<0.001
Intercept	-1.3 ± 1.8	0.5	-74 ± 10	<<0.001	-63 ± 5	<<0.001
	Value	**p-value**	**Value**	**p-value**	**Value**	**p-value**
F-statistic	21.8	<<0.001	19.5	<<0.001	39.1	<<0.001
Adjusted r^2	0.60		0.48		0.74	
LASSO regression parameter	**Coefficient (‰)**		**Coefficient (‰)**		**Coefficient (‰)**	
Surface area (log)	-0.25		–		2.5	
Watershed area (log)	-0.43		-1.6		0.6	
Elevation	-0.006		–		0.023	
Intercept	-6.9		-116		-46	

Table S3. Slope values of daily isotopic change for Lake Potato and Power Lake. Data derived from frequent water samples taken over summer 2018.

	Lake Potato			*Power Lake*		
	$\delta^{18}O$ (‰ d^{-1})	$\delta^{2}H$ (‰ d^{-1})	*dxs* (‰ d^{-1})	$\delta^{18}O$ (‰ d^{-1})	$\delta^{2}H$ (‰ d^{-1})	*dxs* (‰ d^{-1})
Maximum	0.13	0.78	0.04	0.00	0.39	0.07
Minimum	0.00	-0.09	−0.26	0.00	0.00	−0.14
Mean ± 95% CI	0.06±0.05	0.32±0.32	−0.12±0.11	0.02±0.02	0.16±0.18	−0.04±0.07